

Janus-like asymmetrically oxidized graphene: Facile synthesis and distinct liquid crystal alignment at the oil/water interface

Zejun Zhang, Jinli Qin, Huailing Diao, Shasha Huang, Jin Yin, Hui Zhang, Yongxin Duan^{**}, Jianming Zhang^{*}

Key Laboratory of Rubber-Plastics, Ministry of Education/Shandong Provincial Key, Qingdao University of Science & Technology, Qingdao City, 266042, People's Republic of China

ARTICLE INFO

Article history:

Received 13 November 2019

Received in revised form

15 January 2020

Accepted 22 January 2020

Available online 23 January 2020

ABSTRACT

Janus graphene oxide (GO) usually refers to a unique two-dimensional material with asymmetric surface chemistries on opposite faces of the sheets. Herein, we propose a facile and efficient method to fabricate Janus-like GO (JGO) with a novel asymmetric structure along the faces of the sheets. Unlike the traditional post-synthesis of double-faced Janus GO based on pre-prepared GO, the novel JGO with a randomly distributed asymmetric oxidation structure along the sheet face can be achieved by a simple ultrasonic treatment on partially oxidized graphene. The asymmetric oxidation structure along the sheet face of our Janus GO was confirmed by confocal micro-Raman imaging and analysis of height profiles by atomic force microscopy. Due to the asymmetric oxidation structure, the as-prepared JGO has amphiphilic characteristics, with hydrophilicity on one side of the sheet and hydrophobicity on the other side, leading to an eyelash-like liquid crystal alignment at the oil/water interface. The perpendicular alignment rather than the parallel orientation behavior of GO liquid crystals at the oil/water interface further confirms the asymmetric structure of our JGO along the face graphene sheets. The simple approach and a new class of JGO proposed herein provide a new insight into understanding the asymmetric chemistry of graphene.

© 2020 Elsevier Ltd. All rights reserved.

1. Introduction

Janus particles, named after the double-faced Roman god due to their two sides with different compositions or properties [1], have attracted tremendous attention in recent years due to their asymmetric structures, novel performances, and diverse potential applications [2–6]. Numerous multi-dimensional Janus nanomaterials have been prepared in the last decade such as zero-dimensional Janus spheres [7–9], one-dimensional Janus cylinders [10–12], and two-dimensional (2D) Janus nanosheets [13–15]. Among the various 2D nanomaterials reported to date, graphene and its derivatives, especially the water-soluble precursor, graphene oxide (GO), are excellent candidates to prepare 2D Janus nanomaterials. This is because of their unique 2D structures, large surface areas, and advantageous properties [16,17]. For example, graphene Janus sheets exhibit unique properties where the chemical decorations on one

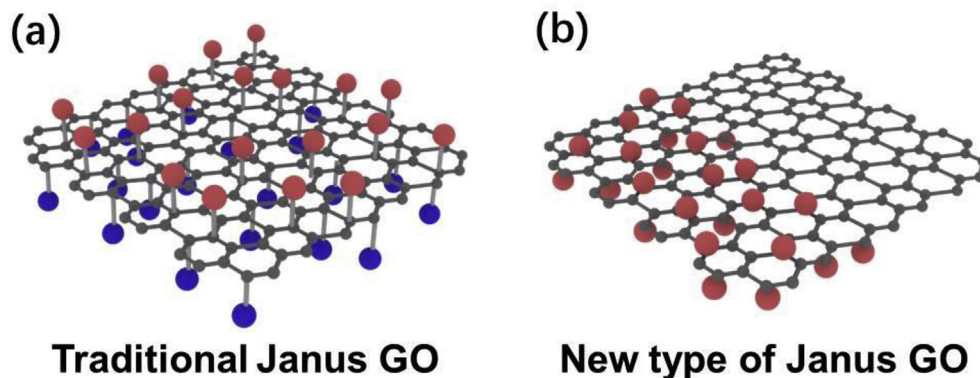
face are capable of affecting the properties on the opposite face, and this has been attributed to the extremely thin nature of the material [18].

To achieve asymmetrical modification on opposite faces of the graphene sheets as illustrated in Scheme 1a, template-assisted strategies have been used to isolate one face while protecting the other; these methods allow chemical modifications to be applied only on the exposed face of the sheets [19]. As an example, Zhang et al. reported the first experimental realization of asymmetrically-modified Janus graphene by a two-step surface covalent functionalization assisted by a poly(methyl methacrylate)-mediated transfer approach [18]. However, the yield of Janus nanosheets achieved using this method was limited by the number of inert templates. To address this efficiently, site-specific modification of Pickering emulsions has been proposed to create Janus nanosheets due to the facile preparation of Pickering emulsions and the fact that emulsion droplets tend to have large surface areas [20,21]. In addition, Leon et al. fabricated Janus nanosheets by combining a Pickering-type emulsion and grafting from polymerization by atom transfer radical polymerization [22]. More specifically, GO nanosheets were

* Corresponding author.

** Corresponding author.

E-mail addresses: dyx@qust.edu.cn (Y. Duan), zjm@qust.edu.cn (J. Zhang).



Scheme 1. Illustration of the different asymmetric chemical structures of (a) traditional Janus GO with different chemical natures on the opposite faces of the sheet, and (b) the new type of Janus GO, exhibiting different chemical properties on opposite sides along the sheet.

initially assembled onto wax beads by Pickering emulsion, then PMMA was grafted selectively from the exposed face [22]. Although elaborate designs for the above template-assisted strategies are known, they generally require complicated and tedious chemical modification process to achieve asymmetrical functionalization on opposite faces of the GO sheets. The development of a facile and efficient method for fabrication of the Janus GO nanosheets therefore remains a challenge. Moreover, during chemical modification, GO tends to aggregate due to the destruction of the electrostatic interactions between sheets [23], thereby rendering the preparation of monolayer Janus GO particularly challenging. We also note that the majority of previous works have focused on asymmetric surface chemistries on opposite sheet faces (Scheme 1a) [24–27], with asymmetric structures along the sheet faces (Scheme 1b) having yet to receive attention. We therefore surmised that if a Janus GO can be synthesized by regulating the degree of oxidation on opposite sides along the sheet, then a monolayer Janus GO with asymmetric amphiphathy could be obtained without further chemical decoration.

Thus, herein we demonstrate a rapid, facile, and efficient method for the fabrication of an asymmetrically oxidized GO exhibiting similar surface structure with that depicted in Scheme 1b. Owing to this method is based on a simple ultrasonic fracture of partially oxidized graphene, the functionalized region of GO is randomly distributed and could not be controlled precisely. We therefore named it as Janus-like GO (JGO). The asymmetric oxidation structure was verified on specific individual sheets through height difference analyses with atomic force microscopy (AFM) and confocal micro-Raman imaging technique. Interestingly, the as-prepared JGO forms an eyelash-like liquid crystal alignment at the oil/water interface. This work therefore demonstrates the use of powerful characterization methods (i.e., AFM height difference analysis and micro-Raman chemical imaging) for direct confirmation of asymmetric oxidation in the monolayer nanosheet. This novel asymmetric structure would be expected to provide a new type of platform for future theoretical and experimental studies of GO.

2. Experimental section

2.1. Synthesis of JGO and GO

The asymmetrically-structured JGO was synthesized through low-dose oxidant peroxidation and strong sonication. More specifically, pre-oxidized graphite (POG) was obtained via a conventional intercalation process using a strong acid and a strong

oxidizing agent. KMnO_4 (2 g, 1 wt equiv.) and natural graphite (1 g, 1 wt equiv., 180 mesh) were added to concentrated H_2SO_4 (2 L, 98%) over a period of 6 h in an ice water bath. After the reaction, the mixed solution was slowly poured into ice water (500 mL) to avoid a sudden increase in temperature, and 30 wt% H_2O_2 was added dropwise until bubbles were no longer produced. The wet POG powder was obtained after filtration with a 400 mesh press cloth and washing until reaching a neutral pH. This wet POG powder was then added to deionized water (400 mL), and the pH of the solution was adjusted to 11 using ammonia water then subjected to sonication for 5 min using an ultrasonic homogenizer with an output power of 180 W (20 mm probe tip diameter, JY92-IIDN, Ningbo Scientz Biotechnology Co. Ltd., China). A monolayer JGO suspension was obtained via further dilution and centrifugation at 8000 rpm for 10 min.

The GO was prepared from natural graphite with a particle size of 180 mesh using the modified Hummers' method [28]. The synthesized GO was suspended in deionized water and subjected to dialysis until a neutral pH was reached, and then gradient centrifugation was carried out at 9000 rpm for 30 min. The resulting well-exfoliated GO sheets had a thickness of approximately 1.2 nm. The purified GO suspension was then dispersed in water to a concentration of 0.2 mg/mL.

2.2. Procedure for preparation of the Pickering emulsion

The Pickering emulsion was prepared using JGO (5 mL) and an equal volume of paraffin. The mixture was stirred for 2 min at 25 °C using a magneton set at 2400 rpm. The pH of the paraffin–water emulsion was controlled by adding 0.1 M HCl or NaOH. The resulting Pickering emulsion was allowed to stand at ambient temperature for at least 24 h. As a control, the Pickering emulsion using GO was also prepared under identical conditions.

2.3. Characterization of JGO

AFM images were acquired using the appropriate probes (SCANASYST-AIR) and a Dimension Icon instrument (BRUKER) under the peak force tapping mode. Dilute JGO suspensions (~1 mg/mL) were spin-coated on a mica substrate at 2000 rpm for 1 min prior to the AFM and Raman measurements. Raman mapping was carried out using an InVia Series Laser Confocal Micro Raman Spectrometer (RENISHAW) using the following settings: $1 \times 1 \mu\text{m}$ pixels, $100 \times$ objective, 532 nm laser with 5% power, diffraction grating of 1800 gr mm^{-1} , 3 s exposure time, 1 accumulation. Transmission electron microscopy (TEM) images were obtained using a JEOL

JEM-2200 FS electron microscope at 200 kV. The samples were prepared on copper grids using Lacey Support Film by diluting the emulsion to obtain a translucent drop.

UV–vis absorption spectra of the JGO suspension were collected in the range of 200–800 nm using a UV–vis spectrophotometer (Shimadzu UV-2550). X-ray photoelectron spectroscopy (XPS) measurements were performed using a Thermo Scientific ESCALAB 250XI photoelectron spectrometer with Al K α radiation (1486.6 eV) as the X-ray source. Wide-angle X-ray diffraction (XRD) patterns were collected at 25 °C on a Rigaku UltimaIV diffractometer with Cu K α radiation ($\lambda = 0.154$ nm), and the diffraction signals were recorded in the range of $2\theta = 5$ – 40° at an interval of 0.05° and a scan rate of 5° min^{-1} .

The Zeta potential of the JGO suspension was measured by dynamic light scattering (NanoBrook Omni, U.S.). Polarized optical microscopy (POM) images were obtained using a Nikon H600L polarized optical microscope equipped with a MD50 CMOS camera. For the POM observations, the sample was dropped onto a glass slide.

3. Results and discussion

3.1. Preparation of JGO

Fig. 1 shows a schematic illustration of the method of preparation employed for JGO, where the synthetic process can be seen to consist of two major stages, i.e., partial oxidation (PO) and fracture exfoliation (FE). In its XRD spectrum, pristine graphite shows a strong peak at 26.3° corresponding to an interlayer distance of approximately 0.33 nm (Fig. S1). This is supported by Raman spectroscopy, where the I_D/I_G ratio region (0.07–0.12) of pristine graphite is low due to the presence of intact π - π conjugated structures (Figs. S2a and S2b). It is well known that oxidation preferentially takes place on the edge and defect sites of graphite due to their higher reactivity. In the PO stage, after low-temperature (0 °C) and low-dosage oxidant (i.e., double the quantity of graphite) treatment, the π - π conjugated structures of the graphite edges were destroyed, and the interlayer spacing of the partial oxidized graphite (POG) increased due to the production of oxygen-containing functional groups. We note there that POG shows a strong peak at 24.1° in the XRD pattern corresponding to an interlayer distance of approximately 0.37 nm, while the weak peak at 31° was attributed to the presence of KMnO_4 and H_2SO_4 (Fig. S1). As shown in Figs. S2c and S2d, the I_D/I_G ratio of the internal region of the POG (~ 0.77) is lower than that of the edges (~ 1). Similar to the action of an inert template, the internal region of POG is protected. The gradient of the degree of oxidation observed was caused by the gradual depletion of the oxidant, from the edges to the interior, during the process. In the following FE stage, the POG

was further broken, and was found to peel off under strong sonication conditions. Due to the randomness of the fractures, a series of JGO species with randomly distributed asymmetric oxidation structure along the sheets was obtained. Some uniformly oxidized layers could also be produced during the process of random ultrasonic breaking. The proportion of sheets with different structures is analyzed in detail in section 3.2.

3.2. Characterization of JGO

3.2.1. Morphologies and asymmetric microstructure

The nature of the JGO prepared with an asymmetric degree of oxidation was assessed by height difference analyses using AFM and micro-Raman imaging. It is well known that oxygen-containing functional groups increase the thickness of graphene nanosheets. In general, the thickness of a monolayer graphene nanosheet is approximately 0.6–0.8 nm due to the presence of few oxygen-containing functional groups [29–31], while the thickness of a monolayer GO nanosheet is approximately 0.9–1.3 nm due to the presence of abundant oxygen-containing functional groups [32–34]. To accurately determine the microscopic chemical structure of the prepared Janus GO, we selected two typical JGO nanosheets to characterize the oxidation degree distribution, and the overall thickness of the isolated JGO was obtained from 4 AFM height profiles. As shown in Fig. 2a–c, the JGO nanosheet showed a significant height difference in the direction of oxidation due to different degrees of oxidation, thereby confirming our previous conjecture. We visually expressed the differences in oxidation degree on the nanosheets as shown in the figure insets. In addition, as can be seen in Fig. 2d, the asymmetric distribution of the oxidation degree becomes more obvious by adjusting the height color scales of the AFM images. In contrast, the overall thickness of the GO is approximately 1.2 nm, indicating a uniform oxidation degree (Fig. S3). It should also be noted that some sheets exist that possess no obvious height difference during the ultrasonic process. Thus, to further verify the asymmetric oxidation degrees of the nanosheets, the JGO and GO samples were characterized by Raman imaging. It is generally accepted that the intensity ratio between the D- and G-bands indicates the structural disorder of the graphene layer [35,36]. In this context, I_D/I_G 2D mapping showed that the JGO nanosheet differed significantly from the GO sample, the latter of which exhibits a uniform color (Figs. 2e, 2g, S4, and S5). In addition, Fig. 2f and h indicate that the JGO had a low I_D/I_G ratio (~ 0.72) in the blue area (low oxidation) and a high I_D/I_G ratio (~ 1.07) in the red area (high oxidation), which differs significantly from that of GO (i.e., ~ 1.02 for the whole area). This is consistent with the observations from AFM measurements.

The asymmetric oxidation may endow the JGO surface having both hydrophobicity and hydrophilicity. To identify the amphiphilic

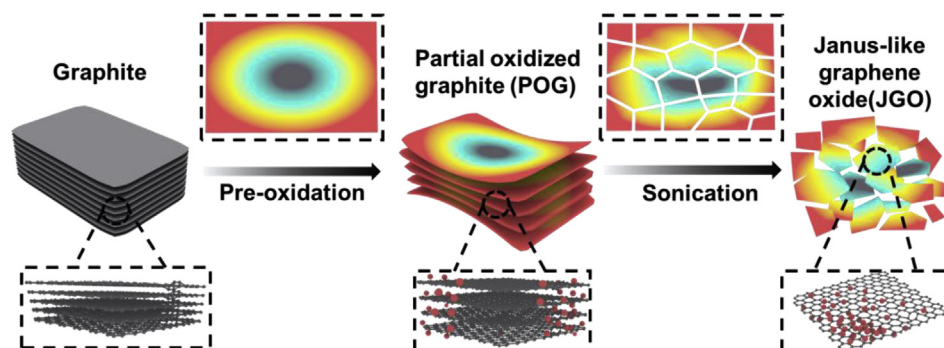


Fig. 1. Schematic illustration of the preparation of JGO. (A colour version of this figure can be viewed online.)

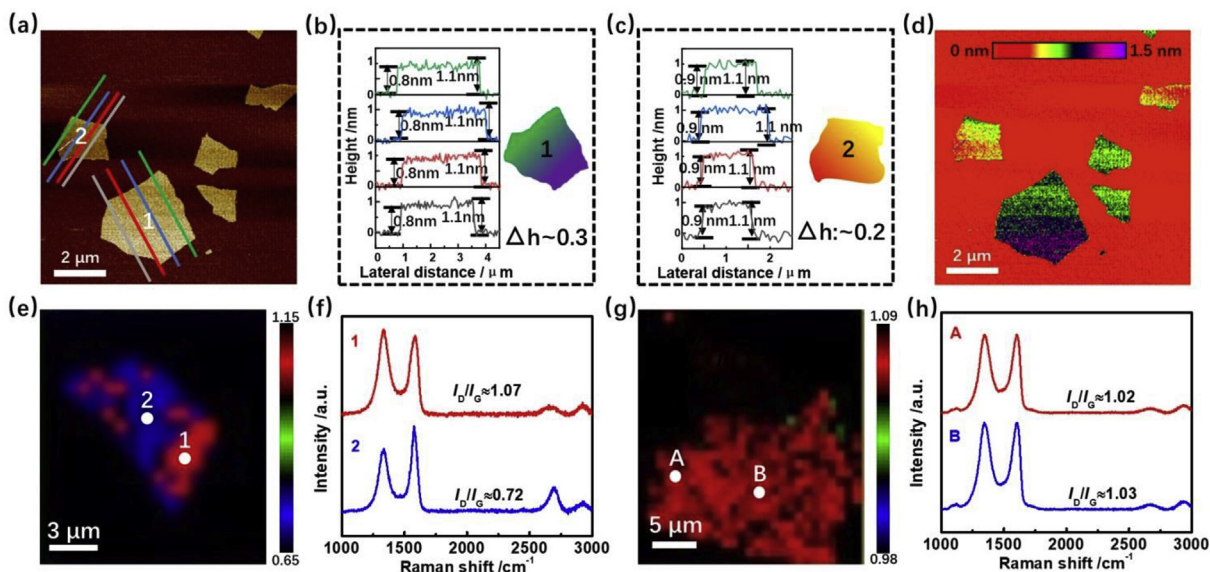


Fig. 2. Morphology studies of JGO and its comparison with traditional GO. (a–d) AFM images of JGO (a) and corresponding height profiles (b, c). The inset diagrams shown in parts (b) and (c) represent the asymmetric oxidation of JGO sheets 1 and 2 as indicated in (a), respectively. (d) The height chromatic aberration image of (a). (e–h) Raman mapping of a JGO sheet (e) and GO (g) using the I_D/I_G ratio from the corresponding Raman spectra (f, h). (A colour version of this figure can be viewed online.)

characteristic of JGO, the interfacial behavior of JGO and traditional GO in the toluene/water system was compared (Fig. S6). It was found that the amphiphilic JGO accumulated at the toluene/water interface while the traditional GO stayed only in the water phase after ultrasonic pretreatment. This result indicated that our JGO indeed has the amphiphilic character.

It should be noted that although long-term ultrasonication is beneficial for sheet exfoliation, the reduction in sheet size cannot be ignored. As shown in Fig. 3a–h, we investigated the lateral size of JGO under a range of ultrasonication times, and statistical analysis of an average of 30 sheets shows that the lateral size decreased upon increasing the ultrasonication time. Furthermore, we also analyzed the height differences of 30 sheets to determine the average degree of asymmetry (Fig. 3i–l, S7). By comparison, we

found that large layers tend to show high levels of asymmetry. As the sizes of the sheets decrease, their asymmetric degree of oxidation decreased gradually, which becomes more obvious with an ultrasonication time of 10 min. After a comprehensive comparison, we determined that the lateral size and levels of asymmetry obtained upon ultrasonication for 5 min were relatively moderate. Based on these observations, subsequent experiments were conducted on JGO fabricated under ultrasonication for 5 min.

3.2.2. Bulk chemical and physical properties

The composition and characteristics of the prepared JGO were evaluated by XPS, UV–vis absorption spectroscopy, and XRD. To obtain detailed information, we used GO for comparison. Thus, Fig. 4a shows the fitted C1s spectra of the JGO and GO membranes.

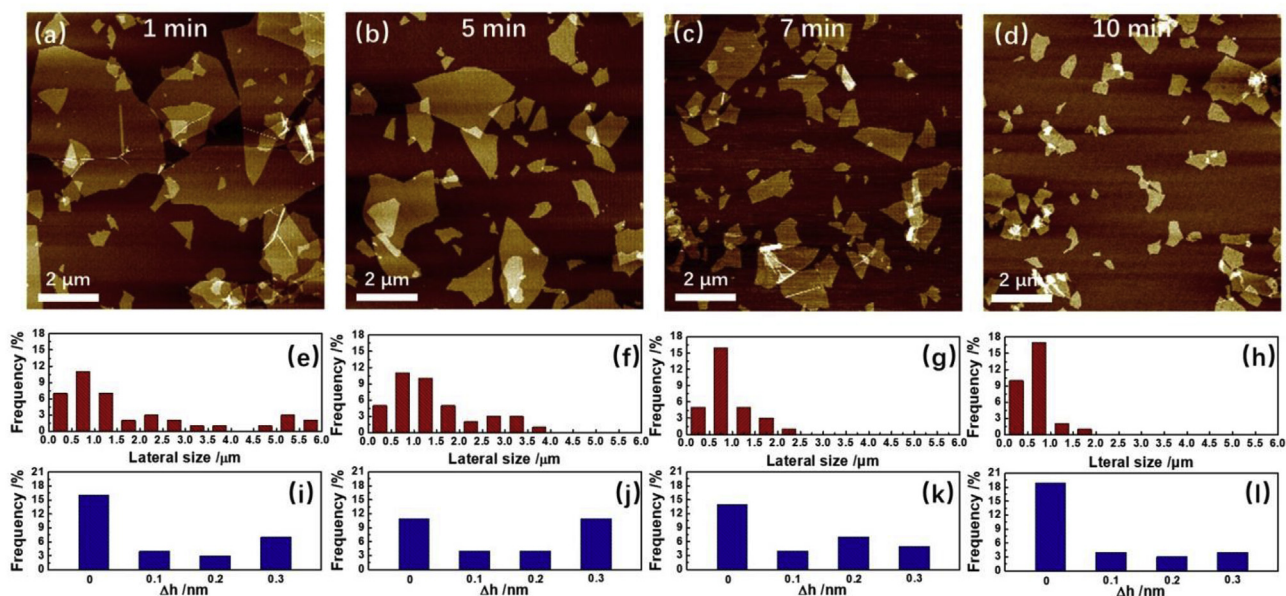


Fig. 3. Effect of sonication time on the size and asymmetric height difference of the as-prepared GO. (a–d) AFM images of the GO sheets obtained under different sonication times; (e–h) Corresponding lateral size histograms, and (i–l) height difference histograms. (A colour version of this figure can be viewed online.)

Compared with GO, the overall oxidation degree of JGO is reduced due to the area of low oxidation on the isolated sheet. As a result, the peak intensity corresponding to C–OH bonds (286.5 eV) for JGO decreases. In addition, the full-width at half-maximum (FWHM) of the sp^2 C bond peak decreases from 1.10 to 0.87 eV, thereby confirming the presence of more ordered sp^2 C structures [37]. This is consistent with the UV–vis observations (Fig. 4b). Furthermore, GO presents a strong absorption peak at 228 nm (π - π^* transition of aromatic C–C bonds) and a weak shoulder peak at \sim 300 nm (n - π^* transition of C=O bonds). Moreover, the strong absorption peak of JGO is up-shifted to 239 nm due to the presence of a more ordered conjugated system [38]. The XRD patterns of JGO and GO films (Fig. 4c) show peaks at $2\theta = 11.3^\circ$ and 10.9° with corresponding interlayer d-spacings of 0.78 and 0.82 nm, respectively. This suggests that the JGO sheets are stacked more tightly than the GO sheets. It should also be noted that the FWHM of JGO increases from 1.24 to 2.15 eV. This wider FWHM compared to that of GO confirms the disordered dispersion of JGO sheets originating from the asymmetric degree of oxidation [39].

3.3. Interface self-assembly behavior of JGO

Pickering emulsions are solid colloidal emulsions stabilized by solid particles in place of organic surfactants, and they can substitute classical emulsions in the majority of emulsion applications, such as in foods, cosmetics, and pharmaceuticals [40–44], and especially in areas where hazardous organic surfactants are unwelcome. The as-prepared JGO exhibits amphiphilic characteristics, with hydrophilic properties on one side and hydrophobic properties on the other side. Similar to conventional amphiphilic surfactants, these are also likely to accumulate and self-assemble into ordered packing structures perpendicular to the oil–water interface; this leads to the formation of a structure with a hydrophilic side in the water phase and a hydrophobic side in the oil phase. In contrast, conventional GO sheets should form stacked layers parallel to the oil–water interface in an emulsion [45]. Thus, the different self-assembly orientation modes for JGO and conventional GO are illustrated in Fig. 5a. To confirm this speculation, high concentrations (2 mg/mL) of JGO and conventional GO were used to stabilize a liquid paraffin-in-water mixture via Pickering emulsions. These two types of emulsions were observed by polarized optical microscopy (POM) between crossed polarizers (Fig. 5a). For both cases, the self-assembled liquid crystal (LC) behaviors have been clearly observed at the oil/water interface. However, the orientation of the LC texture looks totally different. JGO formed an eyelash-like liquid crystal alignment, while GO sheets were self-assembled into the layered LCs around the oil/water interface. In general, the layered LC texture observed by POM are attributed to parallel orientation packing of GO along the oil/water

interface. Thus, the eyelash-like LC alignment may suggest that there is vertical orientation for JGO at the oil/water interface. To further clarify the vertical arrangement of the JGO at the oil–water interface, a polyurethane–water Pickering emulsion was prepared using polyurethane as the oil phase and JGO as the emulsifier. Owing to the good curing crosslinking capability of polyurethane, the self-assembled structure of JGO at the oil/water interface was likely to be preserved. As seen from TEM images (Fig. S8), the vertical arrangement of JGO around the polyurethane particles could be identified clearly. This observation confirmed that the eyelash-like liquid crystal orientation of JGO was resulted from its vertical orientation at the oil/water interface. In addition, the eyelash-like LC orientation of JGO was greatly affected by the concentration (Fig. S9). More specifically, upon increasing the concentration of JGO, the behavior of the interfacial LC becomes more obvious.

To further study the interfacial LC behavior of JGO in emulsions with different oil–water ratios, liquid paraffin-in-water emulsions were prepared using the different oil volume fractions. As shown in Fig. S10a, oil volume fractions (ϕ_o) \leq 0.67 resulted in an increase in the emulsion volume fraction, while an opposite trend was observed with $\phi_o >$ 0.67. In all oil–water ratios, only the oil-in-water emulsions and no water-in-oil can be formed as identified by the dilution test [46]. We selected three typical oil–water ratios ($\phi_o = 0.2, 0.67$ and 0.8) to investigate the interfacial self-assembly behavior of JGO. It was found that JGO could form an eyelash-like liquid crystal alignment at the oil/water interface in all cases (Fig. S10b). We speculated that there are two reasons why JGO can only form oil-in-water emulsion. On the one hand, the three-phase contact angle of JGO film is \sim 70°, which is more hydrophilic and tends to form oil-in-water emulsion. On the other hand, owing to the difference in the thickness of the hydrophilic side (high oxidized surface) and hydrophobic side (less oxidized surface) of JGO, the interface perpendicular self-assembling of JGO in oil-in-water emulsions with the thicker hydrophilic side pointing to outside (water phase) and thinner hydrophobic side pointing to the inside (oil phase) should form more stable and closely ordering packing than the opposite case in water-in-oil emulsion as illustrated in Fig. S10c.

As shown in Fig. S11, the absolute value of Zeta potential of the GO dispersion increased upon increasing the pH from 2 to 11 due to ionization of the COOH groups, as described previously [37]. Owing to its strong hydrophilicity in high-pH solutions, GO can only stabilize Pickering emulsions at a pH of approximately 2. Compared with GO, the absolute value of the Zeta potential of the JGO dispersions relatively decreases due to the decrease in hydrophilicity, which indicates its suitability for stabilizing Pickering emulsions. Finally, the optical micrographs show that JGO can stabilize Pickering emulsions at pH values between 2 and 10.

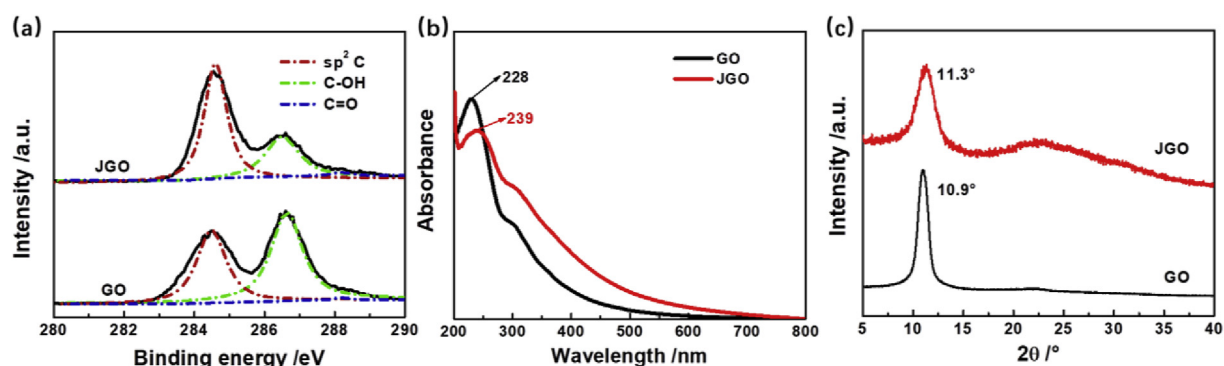


Fig. 4. Characterization of JGO and the conventional GO. (a) C1s XPS spectra of the JGO and GO films. (b) Ultraviolet–visible spectra of the JGO and GO suspensions. (c) Wide angle X-ray diffraction patterns of the JGO and GO films. (A colour version of this figure can be viewed online.)

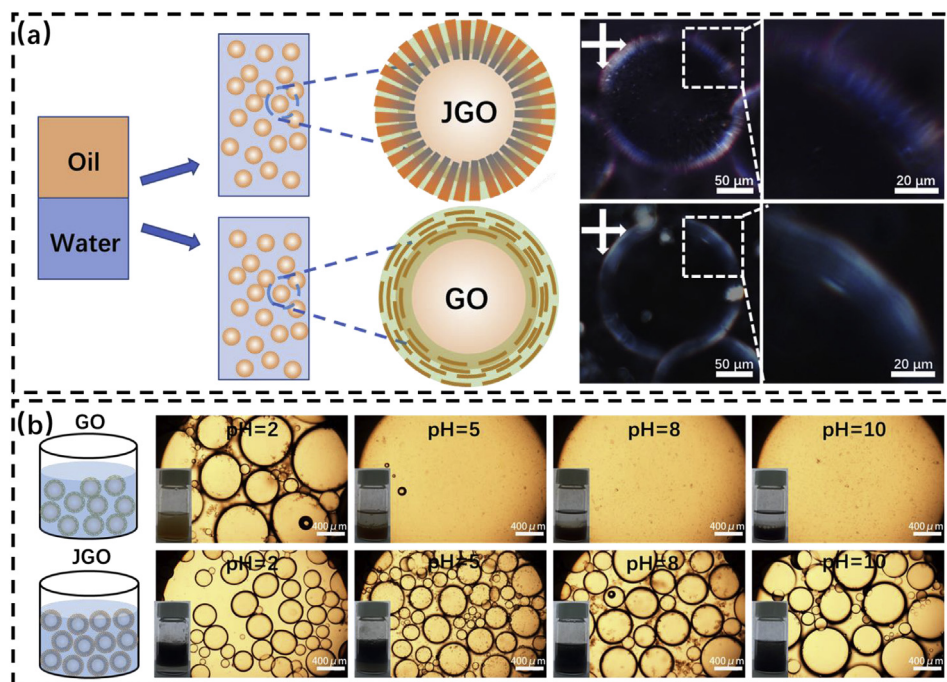


Fig. 5. (a) Schematic illustration of the formation of Pickering emulsion droplets of JGO and GO, and the corresponding POM images of the liquid paraffin-in-water Pickering emulsions stabilized by JGO and GO sheets observed under crossed polarizers (GO and JGO concentrations: 2 mg/mL; oil/water ratio: 1:1; pH = 2). (b) Optical micrographs of liquid paraffin-in-water Pickering emulsions stabilized by GO and JGO at different pH values after standing for 72 h (GO and JGO concentrations: 0.2 mg/mL oil/water ratio: 1:1). (A colour version of this figure can be viewed online.)

4. Conclusions

In conclusion, we herein reported a simple, low-cost, and high-efficiency method for the preparation of Janus-like asymmetrically oxidized graphene by combining partial intercalation oxidation and strong ultrasonic exfoliation. In contrast to the chemical modification of the as-prepared graphene, the preparation and structural regulation of JGO were carried out simultaneously, thereby effectively avoiding the restacking of sheets during the modification process. In addition, it was found that the JGO sheet bearing an asymmetric degree of oxidation was thinner than symmetrically-modified GO. Furthermore, the asymmetric surface chemistries of the JGO nanosheets were confirmed by evaluating their chemical compositions, morphologies, and structural properties. The prepared JGO were also found to exhibit an excellent oil-water interfacial stability due to its unique amphipathicity. Moreover, for the first time, we observed that JGO formed an eyelash-like liquid crystal alignment at the oil/water interface. Since Pickering emulsions can be used as templates to design novel functional hybrid materials [47], this distinct liquid crystal alignment at the oil-water interface paves the way for constructing graphene-based functional materials with novel nanostructures and microstructures.

Declaration of competing interest

The authors declare that they have no known competing financial interests or personal relationships that could have appeared to influence the work reported in this paper.

CRedit authorship contribution statement

Zejun Zhang: Conceptualization, Methodology, Writing - original draft. **Jinli Qin:** Investigation, Resources. **Huailing Diao:** Investigation. **Shasha Huang:** Investigation. **Jin Yin:** Resources. **Hui**

Zhang: Investigation. **Yongxin Duan:** Supervision. **Jianming Zhang:** Supervision, Writing - review & editing.

Acknowledgements

The authors acknowledge the financial support from National Natural Science Foundation of China (51773103, 51603112) and Taishan Mountain Scholar Foundation (TS20081120 and tshw20110510).

Appendix A. Supplementary data

Supplementary data to this article can be found online at <https://doi.org/10.1016/j.carbon.2020.01.078>.

References

- [1] J. Du, R.K. O'Reilly, Anisotropic particles with patchy, multicompartments and Janus architectures: preparation and application, *Chem. Soc. Rev.* 40 (5) (2011) 2402–2416.
- [2] J. Hu, S. Zhou, Y. Sun, X. Fang, L. Wu, Fabrication, properties and applications of Janus particles, *Chem. Soc. Rev.* 41 (11) (2012) 4356–4378.
- [3] S. Jiang, Q. Chen, M. Tripathy, E. Luijten, K.S. Schweizer, S. Granick, Janus particle synthesis and assembly, *Adv. Mater.* 22 (10) (2010) 1060–1071.
- [4] A. Walther, A.H. Muller, Janus particles: synthesis, self-assembly, physical properties, and applications, *Chem. Rev.* 113 (7) (2013) 5194–5261.
- [5] H. Zhou, Z. Guo, Superwetting Janus membranes: focusing on unidirectional transport behaviors and multiple applications, *J. Mater. Chem.* 7 (21) (2019) 12921–12950.
- [6] P.M. Gore, B. Kandasubramanian, Heterogeneous wetttable cotton based superhydrophobic Janus biofabric engineered with PLA/functionalized-organoclay microfibers for efficient oil–water separation, *J. Mater. Chem.* 6 (17) (2018) 7457–7479.
- [7] D. Pan, F. Mou, X. Li, Z. Deng, J. Sun, L. Xu, et al., Multifunctional magnetic oleic acid-coated MnFe₂O₄/polystyrene Janus particles for water treatment, *J. Mater. Chem.* 4 (30) (2016) 11768–11774.
- [8] G.D. Park, J.-K. Lee, Y. Chan Kang, Design and synthesis of Janus-structured mutually doped SnO₂–Co₃O₄ hollow nanostructures as superior anode materials for lithium-ion batteries, *J. Mater. Chem.* 5 (48) (2017) 25319–25327.
- [9] M. Schwarzer, T. Otto, M. Schremp, C. Marschelke, H.T. Tee, F.R. Wurm, et al.,

- Supercooled water drops do not freeze during impact on hybrid Janus particle-based surfaces, *Chem. Mater.* 31 (1) (2018) 112–123.
- [10] A. Walther, M. Drechsler, S. Rosenfeldt, L. Harnau, M. Ballauff, V. Abetz, et al., Self-assembly of Janus cylinders into hierarchical superstructures, *J. Am. Chem. Soc.* 131 (2009) 4720–4728.
- [11] T.M. Ruhland, A.H. Groschel, A. Walther, A.H. Muller, Janus cylinders at liquid-liquid interfaces, *Langmuir* 27 (16) (2011) 9807–9814.
- [12] J. Yan, K. Chaudhary, S. Chul Bae, J.A. Lewis, S. Granick, Colloidal ribbons and rings from Janus magnetic rods, *Nat. Commun.* 4 (2013) 1516.
- [13] W. Chen, Y. Qu, L. Yao, X. Hou, X. Shi, H. Pan, Electronic, magnetic, catalytic, and electrochemical properties of two-dimensional Janus transition metal chalcogenides, *J. Mater. Chem.* 6 (17) (2018) 8021–8029.
- [14] J. Liu, P. Wang, M. Zhou, Y. Ma, X. Niu, G. Pan, et al., Tailored Janus silica nanosheets integrating bispecific artificial receptors for simultaneous adsorption of 2,6-dichlorophenol and Pb (ii), *J. Mater. Chem.* 7 (27) (2019) 16161–16175.
- [15] R. Deng, F. Liang, P. Zhou, C. Zhang, X. Qu, Q. Wang, et al., Janus nanodisc of diblock copolymers, *Adv. Mater.* 26 (26) (2014) 4469–4472.
- [16] Y.B. Tan, J.-M. Lee, Graphene for supercapacitor applications, *J. Mater. Chem.* 1 (47) (2013) 14814–14843.
- [17] T. Yang, H. Lin, K.P. Loh, B. Jia, Fundamental transport mechanisms and advancements of graphene oxide membranes for molecular separation, *Chem. Mater.* 31 (6) (2019) 1829–1846.
- [18] L. Zhang, J. Yu, M. Yang, Q. Xie, H. Peng, Z. Liu, Janus graphene from asymmetric two-dimensional chemistry, *Nat. Commun.* 4 (2013) 1443.
- [19] B.T. McGrail, J.D. Mangalao, B.J. Rodier, J. Swisher, R. Advincula, E. Pentzer, Selective mono-facial modification of graphene oxide nanosheets in suspension, *Chem Commun (Camb)*, 52 (2) (2016) 288–291.
- [20] M. Lattuada, T.A. Hatton, Synthesis, properties and applications of Janus nanoparticles, *Nano Today* 6 (3) (2011) 286–308.
- [21] G. Loget, A. Kuhn, Bulk synthesis of Janus objects and asymmetric patchy particles, *J. Mater. Chem.* 22 (31) (2012) 15457–15474.
- [22] A.C. de Leon, B.J. Rodier, Q. Luo, C.M. Hemmingsen, P. Wei, K. Abbasi, et al., Distinct chemical and physical properties of Janus nanosheets, *ACS Nano* 11 (7) (2017) 7485–7493.
- [23] H. Wu, W. Yi, Z. Chen, H. Wang, Q. Du, Janus graphene oxide nanosheets prepared via Pickering emulsion template, *Carbon* 93 (2015) 473–483.
- [24] A. Holm, J. Park, E.D. Goodman, J. Zhang, R. Sinclair, M. Cargnello, et al., Synthesis, characterization, and light-induced spatial charge separation in Janus graphene oxide, *Chem. Mater.* 30 (6) (2018) 2084–2092.
- [25] D. Luo, F. Wang, B.V. Vu, J. Chen, J. Bao, D. Cai, et al., Synthesis of graphene-based amphiphilic Janus nanosheets via manipulation of hydrogen bonding, *Carbon* 126 (2018) 105–110.
- [26] M. Akbari, M. Shariaty-Niassar, T. Matsuura, A.F. Ismail, Janus graphene oxide nanosheet: a promising additive for enhancement of polymeric membranes performance prepared via phase inversion, *J. Colloid Interface Sci.* 527 (2018) 10–24.
- [27] Y. Yang, L. Zhang, X. Ji, L. Zhang, H. Wang, H. Zhao, Preparation of Janus graphene oxide (GO) nanosheets based on electrostatic assembly of GO nanosheets and polystyrene microspheres, *Macromol. Rapid Commun.* 37 (18) (2016) 1520–1526.
- [28] D.C. Marcano, D.V. Kosynkin, J.M. Berlin, A. Sinitskii, Z. Sun, A. Slesarev, et al., Improved synthesis of graphene oxide[J], *ACS Nano* 4 (8) (2010) 4806–4814.
- [29] M. Matsumoto, Y. Saito, C. Park, T. Fukushima, T. Aida, Ultrahigh-throughput exfoliation of graphite into pristine 'single-layer' graphene using microwaves and molecularly engineered ionic liquids, *Nat. Chem.* 7 (9) (2015) 730–736.
- [30] G. Bepete, E. Anglaret, L. Ortolani, V. Morandi, K. Huang, A. Penicaud, et al., Drummond, Surfactant-free single-layer graphene in water, *Nat. Chem.* 9 (4) (2017) 347–352.
- [31] L. Dong, Z. Chen, X. Zhao, J. Ma, S. Lin, M. Li, et al., A non-dispersion strategy for large-scale production of ultra-high concentration graphene slurries in water, *Nat. Commun.* 9 (1) (2018) 76.
- [32] L. Peng, Z. Xu, Z. Liu, Y. Wei, H. Sun, Z. Li, et al., An iron-based green approach to 1-h production of single-layer graphene oxide, *Nat. Commun.* 6 (2015) 5716.
- [33] X. Fan, W. Peng, Y. Li, X. Li, S. Wang, G. Zhang, et al., Deoxygenation of exfoliated graphite oxide under alkaline conditions: a green route to graphene preparation, *Adv. Mater.* 20 (23) (2008) 4490–4493.
- [34] P. Liu, H. Yang, X. Zhang, M. Jiang, Y. Duan, J. Zhang, Controllable lateral contraction and mechanical performance of chemically reduced graphene oxide paper, *Carbon* 107 (2016) 46–55.
- [35] K.N. Kudin, B. Ozbas, H.C. Schniepp, R.K. Prud'homme, I.A. Aksay, R. Car, Raman spectra of graphite oxide and functionalized graphene sheets, *Nano Lett.* 8 (1) (2018) 36–41.
- [36] L.M. Malard, M.A. Pimenta, G. Dresselhaus, M.S. Dresselhaus, Raman spectroscopy in graphene, *Phys. Rep.* 473 (5–6) (2009) 51–87.
- [37] D. Yang, A. Velamakanni, G. Bozoklu, S. Park, M. Stoller, R.D. Piner, et al., Chemical analysis of graphene oxide films after heat and chemical treatments by X-ray photoelectron and Micro-Raman spectroscopy, *Carbon* 47 (1) (2009) 145–152.
- [38] Q. Zhang, X. Qian, K.H. Thebo, H.-M. Cheng, W. Ren, Controlling reduction degree of graphene oxide membranes for improved water permeance, *Sci. Bull.* 63 (12) (2018) 788–794.
- [39] A. Akbari, P. Sheath, S.T. Martin, D.B. Shinde, M. Shaibani, P.C. Banerjee, et al., Large-area graphene-based nanofiltration membranes by shear alignment of discotic nematic liquid crystals of graphene oxide, *Nat. Commun.* 7 (2016), 10891.
- [40] C.C. Berton-Carabin, K. Schroen, Pickering emulsions for food applications: background, trends, and challenges, *Annu. Rev. Food Sci. Technol.* 6 (2015) 263–297.
- [41] S. Lam, K.P. Velikov, O.D. Velev, Pickering stabilization of foams and emulsions with particles of biological origin, *Curr. Opin. Colloid Interface Sci.* 19 (5) (2014) 490–500.
- [42] J. Tang, P.J. Quinlan, K.C. Tam, Stimuli-responsive Pickering emulsions: recent advances and potential applications, *Soft Matter* 11 (18) (2015) 3512–3529.
- [43] D. Marku, M. Wahlgren, M. Rayner, M. Sjö, A. Timgren, Characterization of starch Pickering emulsions for potential applications in topical formulations, *Int. J. Pharm.* 428 (1–2) (2012) 1–7.
- [44] H. Chen, H. Zhu, J. Hu, Y. Zhao, Q. Wang, J. Wan, et al., Highly compressed assembly of deformable nanogels into nanoscale suprastructures and their application in nanomedicine, *ACS Nano* 5 (4) (2011) 2671–2680.
- [45] W. Wan, Z. Zhao, T.C. Hughes, B. Qian, S. Peng, X. Hao, et al., Graphene oxide liquid crystal Pickering emulsions and their assemblies, *Carbon* 85 (2015) 16–23.
- [46] J. Kim, L.J. Cote, J. Huang, Two dimensional soft material: new faces of graphene oxide, *Acc. Chem. Res.* 45 (8) (2012) 1356.
- [47] W. Yi, H. Wu, H. Wang, Q. Du, Interconnectivity of macroporous hydrogels prepared via graphene oxide-stabilized pickering high internal phase emulsions, *Langmuir* 32 (4) (2016) 982–990.